# Flying at Your Fingertips: Input Mapping Strategies for Fingertip Force-Based 3D Locomotion

Shun Kondoh
The University of Tokyo
Bunkyo, Tokyo, Japan
shun_kondo@cyber.t.u-tokyo.ac.jp

Takeru Hashimoto
The University of Tokyo
Bunkyo, Tokyo, Japan
takeu.hashimoto.research@gmail.com

Yutaro Hirao
Nara Institute of Science and Technology
Ikoma, Nara, Japan
yutarohirao@gmail.com

Takuji Narumi
The University of Tokyo
Bunkyo, Tokyo, Japan
narumi@cyber.t.u-tokyo.ac.jp

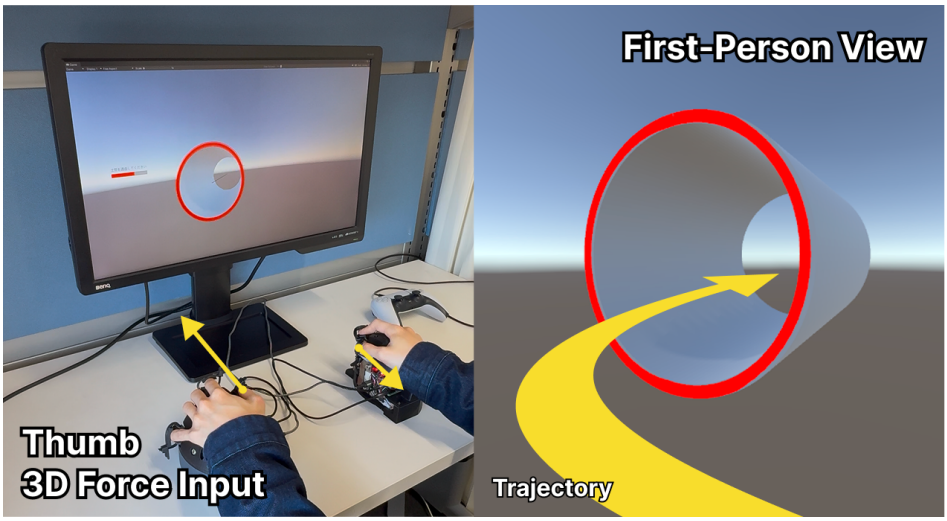


**Figure 1: Evaluation of 3D locomotion control using fingertip force input in this study. Participants used the fingertip force input system YUBI (left) to control 4DoF movement by the magnitude and direction of forces applied with their thumbs, and performed a task of passing through tunnels (right) displayed in a 3D space from a first-person perspective. In this study, we compared five different input mapping strategies to clarify optimal design guidelines for force input devices.**

## Abstract

Achieving intuitive yet precise 3D locomotion remains a challenge in Human Computer Interaction; joystick-based control requires extensive training, while body-motion interfaces suffer from fatigue and spatial constraints. Fingertip force input offers a promising alternative by combining minimal physical displacement with high-dimensional control, yet optimal strategies for mapping force to 3D movement remain unexplored. This study systematically evaluates five mapping strategies for 4DoF locomotion (3 translational axes + yaw) to establish design guidelines for force-based interfaces. Through a tunnel-passing experiment comparing a standard gamepad against four force-input mappings, we demonstrate that directly replicating standard joystick mappings on force devices significantly degrades performance due to inherent cross-axis interference. In contrast, our proposed "wheel-like" redundant mapping, which integrates 6DoF force inputs from both thumbs, achieved performance parity with gamepads while yielding superior ratings for intuitiveness and embodiment. These findings provide a critical design implication: effective force input interfaces should not emulate displacement-based controls but instead leverage redundancy and real-world metaphors to balance precision, intuitiveness, and physical demand.


*AHs 2026, Okinawa, Japan*

ACM ISBN 979-8-4007-2351-3/2026/03
https://doi.org/10.1145/3795011.3795047

## CCS Concepts

• **Human-centered computing** → **Human computer interaction (HCI)**.

## Keywords

Locomotion, Force Input, Input Mapping, Force-Based Input, Drone Control Interface

**ACM Reference Format:**
Shun Kondoh, Takeru Hashimoto, Yutaro Hirao, and Takuji Narumi. 2026. Flying at Your Fingertips: Input Mapping Strategies for Fingertip Force-Based 3D Locomotion. In *The Augmented Humans International Conference 2026 (AHs 2026), March 16–19, 2026, Okinawa, Japan.* ACM, New York, NY, USA, 10 pages. https://doi.org/10.1145/3795011.3795047

## 1 Introduction

The ability to freely navigate through 3D space is becoming increasingly critical for diverse applications, including VR locomotion, drone teleoperation, and remote robot control. In particular, 3D locomotion control for drones is in high demand across fields such as aerial photography, agriculture, and construction [3]. Given their mechanical structure, drones primarily operate with 4DoF (forward/backward, left/right, up/down, and yaw rotation), making the design of effective 4DoF control interfaces a pivotal research subject.

Currently, joystick-based control using remote control (RC) transmitters or game controllers is the mainstream standard. The "Mode 2" configuration, assigning vertical movement and yaw to the left stick, and horizontal translation to the right, has become the de facto standard. However, because a standard joystick provides only 2DoF, designers are forced to distribute the 4DoF movement across two separate sticks. This results in arbitrary mappings where input directions often conflict with output movement directions. For example, the same physical action of tilting a stick "forward" produces different outputs depending on the hand used: the left stick triggers an ascent (vertical), while the right stick triggers forward translation (horizontal). This misalignment between input and output spaces forces users to maintain separate mental models for each hand, significantly increasing cognitive load and necessitating extensive training to master complex multi-axis maneuvers.

To mitigate these high proficiency requirements, alternative interfaces leveraging body movements have been proposed to enhance intuitiveness. Methods using hand and upper body gestures [1, 12, 15, 17–21, 23, 25, 27], foot movements [26], or gaze and head tracking [2, 7, 8, 10, 28] allow users to directly map their intended direction to corresponding body movements (e.g., leaning forward to move forward). While intuitive, these approaches face practical limitations: tracking large body movements requires significant physical space and induces fatigue during extended use. Furthermore, sensor-based tracking can introduce latency and accuracy issues that degrade precise control. This landscape underscores the need for an interface that balances the intuitiveness of body motion with the practicality of stationary controllers.

Fingertip force input interfaces (e.g., YUBI [11]) have emerged as a promising approach to address these challenges. Unlike joysticks that rely on physical displacement (2DoF), force input can sense 3-axis force components (3DoF) per finger without requiring movement. This characteristic offers two key advantages: (1) higher input dimensionality, which allows multiple movement axes to be consolidated onto a single finger, potentially reducing the cognitive load of coordinating two hands; and (2) minimal physical displacement, which mitigates the fatigue and spatial constraints associated with body motion. However, the optimal strategy for mapping these multi-dimensional force inputs to 3D locomotion remains unclear. It is unknown whether traditional joystick mappings can be directly transferred to isometric force input, or if entirely new mapping metaphors are required to fully leverage the device's capabilities.

To address this gap, this study systematically evaluates input mapping strategies for 4DoF locomotion using the fingertip force input system. We compared five conditions: a standard gamepad (Mode 2) and four force-based mapping strategies, including direct joystick emulation and novel metaphorical mappings. Twenty participants performed a tunnel-passing task, and assessed objective performance (time, accuracy, collision), subjective experience (SSQ, VEQ, NASA-TLX) and qualitative data through semi-structured interviews. Our work contributes the first empirical evidence that directly porting joystick mappings to force input degrades performance due to cross-axis interference. Conversely, we demonstrate that a "wheel-like" redundant mapping, integrating bimanual 6DoF inputs, achieves performance comparable to gamepads while significantly enhancing intuitiveness and embodiment. These findings provide critical design guidelines for future force-based 3D locomotion interfaces.

## 2 Related Work

The design of 3D locomotion interfaces requires balancing physical constraints with control fidelity. Existing approaches can be broadly categorized based on the physiological nature of the muscular contraction involved: *isotonic* and *isometric* interaction. Isotonic interfaces rely on physical displacement, where users move a limb or a device through space (Motion-based). In contrast, isometric interfaces capture the force exerted against a rigid surface without significant physical movement (Force-based). In this section, we review these two paradigms and discuss how force-based interaction, particularly when applied to fingertips, offers unique advantages for high-dimensional locomotion.

### 2.1 Joystick-Based and Body Motion-Based Interfaces

The most widely used method for 3D locomotion control is joystick operation using game controllers or RC transmitters. While the standard "Mode 2" mapping provides precise control, it forces users to decompose 4DoF movement into two separate 2DoF inputs. This misalignment between input actions and output movements creates a high cognitive load and necessitates extensive training to master.

To overcome this lack of intuitiveness, numerous interfaces leveraging body movements have been proposed. These methods utilize the "natural mapping" of body parts, such as hand and upper body movements [1, 12, 15, 17, 19–21, 23, 25, 27], foot movements [26], and head movements [2, 7, 8, 10, 28]. For instance, Miehlbradt et al. [18] demonstrated that input mappings based on spontaneous upper-body movements (Body-Machine Interface) significantly reduced learning time compared to joysticks. Similarly, head-based controls like HeadJoystick [8] and others [2] have shown that involving vestibular-aligned movements can enhance sensorimotor congruence, leading to reduced motion sickness and increased presence.

However, these body motion-based methods face inherent practical constraints. First, reliance on camera-based tracking (e.g., Kinect) often introduces sensor latency or occlusion issues that degrade precision [18]. Second, the requirement for large physical movements

limits practicality in confined spaces and induces physical fatigue during extended use [8]. Third, specific modalities like gaze control can conflict with visual observation tasks [18]. These limitations highlight the need for an interface that retains the intuitiveness of body motion while maintaining the compactness and practicality of traditional controllers.

## 2.2 Force Input System

Research into force-based interaction extends beyond simple button presses to capturing user intention directly from muscular exertion. Whole-body systems like "Motion-less VR" [13] utilize torque from restrained limbs to align proprioceptive effort with virtual motion. In contrast, "Tsumori" control [22] focuses on inferring intended actions from discrete force patterns. Recent work on "Motionless Movement" [5] further highlights the potential of using subtle, continuous force input for interaction. Multi-dimensional fingertip force input interfaces [9, 11] offer a compelling approach to making these benefits widely accessible. By consolidating multiple DoFs into single fingertips with minimal physical displacement, they allow for fatigue-free, space-efficient operation (similar to joysticks) while enabling intuitive, multi-axis control (similar to body motion).

Despite these hardware advantages, the optimal input mapping strategy for force-based 3D locomotion remains an open question. Crucially, force input devices differ fundamentally from joysticks: joystick input is displacement-based, where users move the stick by changing finger joint angles, making it relatively easy to isolate input along individual axes. In contrast, force input is *isometric* and requires exerting force without physical displacement, making independent axis control inherently more difficult. Indeed, Li et al. [16] demonstrated that when operating an isometric device, unintended force components arise in non-target directions, confirming cross-axis interference as a fundamental characteristic of isometric input. Despite this challenge, isometric input has shown promise for locomotion control: Cooper et al. [4] found that an isometric joystick achieved superior turning performance compared to a position-sensing joystick in powered wheelchair driving. These findings suggest that isometric force input has potential for locomotion control, but simply applying standard joystick mappings (e.g., Mode 2) may be ineffective due to cross-axis interference. It remains unclear whether force input should mimic established joystick conventions or adopt entirely new metaphors to leverage its high dimensionality.

This study bridges this gap by systematically evaluating mapping strategies for 4DoF locomotion using fingertip force input. We hypothesize that to maximize the potential of force input, mappings must account for its unique physical properties, specifically by utilizing redundancy to mitigate cross-talk. By comparing standard joystick emulation (Mode 2) against novel strategies like a "wheel-based" mapping, we aim to establish design guidelines for the next generation of 3D locomotion interfaces.

# 3 Method

The objective of the experiment is to investigate the suitable mapping of controller input and output motion, which could achieve relatively fast and accurate manipulation with intuitiveness. Therefore, the research question is "what is the optimal input mapping strategy and design guideline that leverages the characteristics of fingertip force input devices to balance precision and intuitiveness in 4DoF 3D locomotion?"

## 3.1 System Design

*3.1.1 Physics-based Player Control.* All player movement was governed by a unified physics simulation implemented in Unity. The player was represented as a rigid body with a spherical collider (radius 0.001 m), a mass of 1.0 kg, and an inertia tensor uniformly set to 1.0. Pitch and roll rotations were constrained to maintain an upright posture, while yaw rotation was permitted.

Player movement was calculated by applying forces and torques to the player rigidbody in each frame. Three translational axes (forward/backward, left/right, up/down) were mapped to world-oriented force vectors based on the player's facing direction, and yaw rotation was mapped to torque around the vertical axis. Upper limits were imposed to maintain consistent motion characteristics across conditions: maximum velocity 6.0 m/s, maximum angular velocity 1.0 rad/s, maximum force 6.0 N, and maximum torque 1.0 N·m.

All control inputs were normalized to the range [0, 1] prior to conversion into physical quantities. Translational commands were multiplied by a translational gain of 6.0, and rotational commands by a torque gain of 1.0, values determined through pilot testing to yield comfortable motion speeds.

*3.1.2 Input Devices.* We compared five input conditions: four force-based input configurations using the YUBI system and one joystick-based condition described below. For force-based input condition, we used the fingertip force input system YUBI [11], which consists of spherical fingertip devices equipped with seven load cells (20 kg max., 80 Hz). YUBI can acquire 14-DoF force input from both thumbs and index fingers (3-DoF each) and little fingers (1-DoF). In this study, only the 6-DoF from both thumbs were used to standardize the modality across conditions and enable direct comparison with joystick operation. YUBI measures both the magnitude and direction of applied fingertip forces without requiring physical displacement.

GamePad operation was included as a conventional baseline. We use Sony PlayStation DualSense controller[1] for the GamePad condition. The required fingertip force for full tilt in the gamepad joystick (approximately 1.4 N) was obtained from the device datasheet and used for normalization, ensuring that equivalent physical effort results in equivalent movement between force input and gamepad condtions.

## 3.2 Apparatus

The experimental system was implemented using Unity 2022.3.8f1 on a desktop PC (CPU: Intel Core i7-13980HX, GPU: NVIDIA GeForce RTX 4080, RAM: 32 GB). The display monitor was an 23.6-inch LCD display (resolution 1920×1080, refresh rate 60 Hz), positioned approximately 60 cm from participants.

[1] https://www.playstation.com/en-us/accessories/dualsense-wireless-controller/

## 3.3 Conditions

This experiment was conducted as a within-participants design. The independent variable was operation condition (5 levels).

To clarify the optimal input mapping strategy for 3D locomotion control using fingertip force input, we established five operation conditions based on the following design principles. First, we adopted conventional joystick operation (gamepad Mode 2) as a comparison baseline. Next, we designed four conditions for force input operation. First, we set up a condition that reproduces mapping similar to Mode 2 for direct comparison with joystick. Second, we established two conditions that separate roles between left and right hands to examine the effect of yaw operation assignment (left hand vs. right hand) on operability. Third, we set up a condition using a wheel metaphor to verify the effectiveness of a more intuitive operation model.

The five operation conditions are as follows:

(1) **GP-M2 (GamePad Mode 2)**: Adopts Mode 2, standard for drone operation. Left stick controls vertical movement and left/right yaw rotation, right stick controls forward/backward movement and left/right translational movement (Figure 2-1).
(2) **YB-M2 (YUBI Mode 2)**: Mapping similar to GP-M2. Left thumb controls vertical movement and left/right yaw rotation, right thumb controls forward/backward movement and left/right translational movement. Each axis is controlled by force input in the corresponding direction (Figure 2-2).
(3) **YB-RY (YUBI Right-Yaw)**: Left thumb controls left/right translational movement, right thumb controls vertical movement, left/right yaw rotation, and forward/backward movement (Figure 2-3).
(4) **YB-LY (YUBI Left-Yaw)**: Left thumb controls left/right yaw rotation, right thumb controls forward/backward movement, vertical movement, and left/right translational movement (Figure 2-4).
(5) **YB-W (YUBI Wheel)**: Mimics wheel motion. Unlike the other conditions that use 4DoF input, YB-W uses all 6DoF (3DoF per thumb) to control 4DoF locomotion. Each thumb's forward/backward force corresponds to the driving force of each wheel; forward motion is the average of both inputs, yaw rotation is the difference (left minus right). Vertical and lateral movements are controlled by the average of upward and lateral forces from both thumbs, respectively (Figure 2-5).

The presentation order of operation conditions was counterbalanced using Latin square design.

## 3.4 Task

The experimental task was a reaching task to pass through cylindrical tunnels arranged in 3D space. This task was designed to evaluate participants' ability to accurately control translational movement to reach the tunnel positions and to perform yaw rotation to align with the tunnel orientations. The player operated by participants was placed at the origin (coordinates (0, 0, 0)) at the start of each trial, beginning facing forward (+Z axis direction). Tunnels were arranged at two height levels (upper layer at 10m, lower layer at -10m), with three horizontal directions at each level (0°, +45°, -45° from the forward direction), resulting in six spatial positions. Each tunnel had an inner diameter of 2m, outer diameter of 2.2m, and length of 3m, with its entrance center positioned at a horizontal distance of 20m from the origin. Additionally, tunnels at each position were rotated by 45° around their axis, creating three orientation variations per position, for a total of 18 tunnel types (2 heights × 3 directions × 3 rotations). The tunnel layout is shown in Figure. 3.

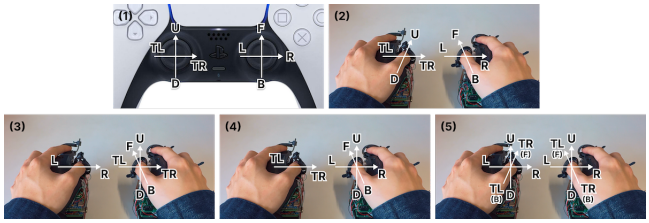


**Figure 2: Input mappings for the five operation conditions. (1) GP-M2, (2) YB-M2, (3) YB-RY, (4) YB-LY, (5) YB-W. F: forward, B: backward, L: left, R: right, U: up, D: down, TL: turn-Left, TR: turn-Right.**

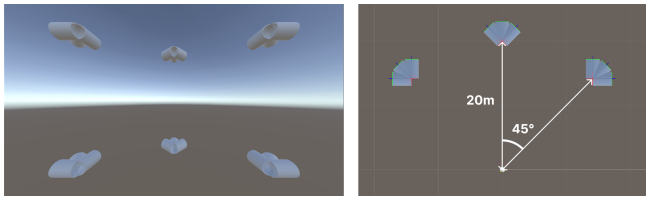


**Figure 3: Tunnel layout. Left: tunnel arrangement as seen from first-person perspective, Right: tunnel arrangement as seen from above.**

In each trial, participants were presented with one target tunnel. Before starting the task, participants were instructed to pass through the tunnel as quickly as possible and to operate so as to pass through the tunnel center. They were also instructed to move parallel to the tunnel to avoid collisions as much as possible. Tunnels had a set entry direction, with the entrance colored red. A centerline was drawn in the tunnel center, serving as a guide for passing through the middle. A reticle was drawn in the screen center, making it easy to grasp the center of the screen.

Each trial proceeded as follows: (1) When the participant relaxes both hands' force below a predefined force threshold from the calibrated zero-point and this state continues for 1 second, the target appears, (2) The participant continues operating until passing through the tunnel or reaching the time limit (15 seconds), (3) After trial completion, the next trial begins.

A success sound was played when passing through the tunnel, and a failure sound was played when exceeding the time limit. If colliding with the tunnel, the screen flashed red and a warning sound was played.

While relaxing force, the magnitude of force input was visually displayed so that participants could confirm their input.

Additionally, a green gauge gradually filled while force was kept below the threshold, the target appeared when it filled for 1 second. Participants were thus instructed not to apply force until the green

gauge filled. Furthermore, a red gauge showing remaining time for each trial was displayed on screen, decreasing as time elapsed.

One set consisted of 18 trials, with 18 types of tunnels presented in random order. Two sets were performed for each operation condition, with calibration performed between sets.

## 3.5 Participants

There were 20 experimental participants (11 males, 9 females, mean age 23.5 years ($SD$ = 7.7), 18 right-handed, 2 left-handed). None of the experimental participants had experience operating drones. Sample size was set at 20, a multiple of 5, considering statistical power and control of order effects through Latin square design. All experimental participants had no prior knowledge of the experimental content. Participants were paid an Amazon gift certificate worth approximately $13 USD as compensation after experiment completion. The experiment duration was approximately 90 minutes.

## 3.6 Procedure

This study was approved by the research ethics committee of the authors' university. Experimental participants first received an explanation of the experiment's purpose and procedure, and written consent to participate was obtained. They then responded to a questionnaire on basic information and the Simulator Sickness Questionnaire (SSQ) [14] to evaluate pre-experiment sickness.

Next, experimental participants received detailed explanations of the force input system overview and experimental tasks. Then, according to one of the five operation conditions, they wore the force input device or held the controller. When wearing the force input device, they tightened it to the extent that thumbs would not slip out and confirmed they could push and pull forward and backward. With assistance from an experimenter, they confirmed operation methods and experientially understood input-output correspondence relationships.

After calibration was performed, the task was started. Two sets (36 trials total) were performed for one operation condition. Calibration was performed between each set to correct input drift.

After tasks for one operation condition were completed, experimental participants removed the device and responded to SSQ, Agency items from the Virtual Embodiment Questionnaire (VEQ) [24], and the localized version of NASA Task Load Index (NASA-TLX) [6].

This procedure was repeated for all five operation conditions. Participants were allowed to take breaks at any time during the experiment as needed.

After experiments for all operation conditions were completed, experimental participants underwent semi-structured interviews. After completing compensation procedures, the experiment was concluded.

## 3.7 Measurements

In this study, we collected behavioral logs as objective measures and questionnaires and interview data as subjective measures.

*3.7.1 Behavioral Logs.* The following data were recorded as logs for each frame: participant ID, operation condition, set number, trial number, target tunnel ID, experiment state, player position (x, y, z coordinates), player rotation angle around y-axis, player velocity (3-axis components and magnitude), collision state with tunnel, input values (for GP-M2, left and right stick input values for 2 axes each; for force input conditions, left and right thumb force input values for 3 axes each), and force applied to the player (3-axis components and magnitude). At trial completion, completion time, distance from tunnel center, passing angle, passing speed, incident angle, etc. were recorded separately. From these data, we calculated measures such as completion time, passing position accuracy, average velocity, maximum velocity, and collision count for each trial.

*3.7.2 Subjective Measures.* SSQ was conducted before the experiment and after each operation condition to evaluate the degree of simulator sickness. NASA-TLX was conducted after each operation condition, evaluating six items—Mental Demand, Physical Demand, Temporal Demand, Performance, Effort, and Frustration—on a 7-point Likert scale. We used Agency items from VEQ to evaluate the sense of embodiment for operation.

*3.7.3 Semi-structured Interview.* After experiencing all operation conditions, semi-structured interviews were conducted. The final interview questions were as follows:

- Which operation method felt most intuitive? Why?
- Which operation method was easiest to operate? Why?
- Which operation method felt most difficult? Why?
- Did you have any strategy when heading toward targets?
- Did you experience any difficulties or confusion during operation?

# 4 Results

## 4.1 Tunnel Pass Count

We counted the number of tunnels each participant successfully passed through in each operation condition. Thirty-six trials (2 sets × 18 tunnels) were performed for each operation condition, and trials that passed through tunnels within the time limit were counted as successes. Wilcoxon signed-rank tests with Shaffer correction revealed: GP-M2 ($M$ = 20.70, $SD$ = 10.12) > YB-M2 ($M$ = 4.35, $SD$ = 5.63, $p < .001$), YB-W ($M$ = 21.35, $SD$ = 11.26) > YB-M2 ($p < .001$), YB-LY ($M$ = 14.10, $SD$ = 11.60) > YB-M2 ($p = .003$), YB-RY ($M$ = 15.25, $SD$ = 11.03) > YB-M2 ($p = .010$), GP-M2 > YB-LY ($p = .048$), YB-W > YB-RY ($p = .018$). Results are shown in Figure 4.

## 4.2 Task Completion Time

For trials with successful tunnel passage, we measured time from trial start (target appearance) to tunnel passage and calculated mean completion time for each participant in each operation condition. Shapiro-Wilk test results confirmed normality for all conditions (all $p > .05$). Paired t-tests with Shaffer correction revealed: GP-M2 ($M$ = 11.24, $SD$ = 1.23) > YB-W ($M$ = 9.75, $SD$ = 1.29, $t(18) = 4.19$, $p = .006$, $d = 0.96$), YB-RY ($M$ = 10.88, $SD$ = 1.56) > YB-W ($t(17) = 3.09$, $p = .040$, $d = 0.73$). Results are shown in Figure 5.

## 4.3 Jerk Integral

To evaluate movement smoothness, we calculated integrated jerk magnitude (time derivative of acceleration) during trials. For trials with successful tunnel passage, we calculated mean jerk integral

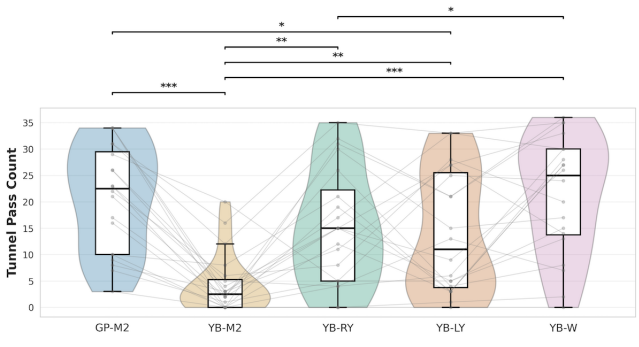


**Figure 4: Tunnel pass count for each operation condition. Shows violin plots and box plots, as well as trajectories for each participant. Pairs with significant differences are shown with lines and asterisks (*: $p < .05$, **: $p < .01$, ***: $p < .001$).**

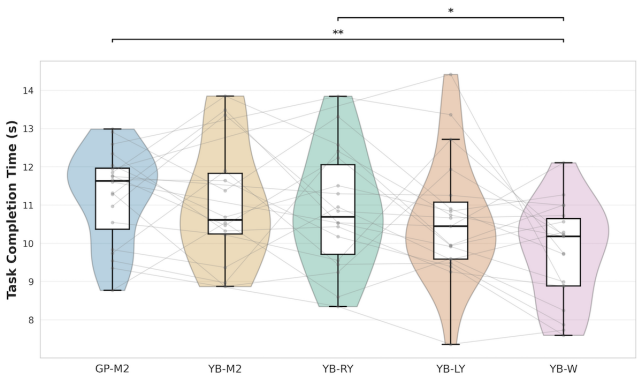


**Figure 5: Task completion time for each operation condition. Shows violin plots and box plots, as well as trajectories for each participant. Pairs with significant differences are shown with lines and asterisks (*: $p < .05$, **: $p < .01$).**

for each participant in each operation condition. Shapiro-Wilk test results rejected normality for GP-M2 ($W = 0.87$, $p = .011$) and YB-M2 ($W = 0.86$, $p = .008$), so we used non-parametric tests. Wilcoxon signed-rank tests with Shaffer correction revealed: YB-M2 ($M = 4578.70$, $SD = 1195.08$) > YB-W ($M = 3442.00$, $SD = 1318.17$, $p < .001$), GP-M2 ($M = 4283.27$, $SD = 1164.81$) > YB-W ($p < .001$), YB-M2 > YB-LY ($M = 4001.14$, $SD = 1249.83$, $p = .002$), YB-RY ($M = 4129.93$, $SD = 1338.26$) > YB-W ($p = .029$), YB-LY > YB-W ($p = .029$). Results are shown in Figure 6.

## 4.4 SSQ (Simulator Sickness Questionnaire)

We used SSQ to evaluate the degree of simulator sickness before the experiment and after all operation conditions. We analyzed changes in Total Severity score before and after the experiment. Pre-experiment Total Severity score was $M = 5.42$ ($SD = 6.81$), post-experiment was $M = 8.60$ ($SD = 14.16$). Shapiro-Wilk test on the difference (post-experiment - pre-experiment) rejected normality

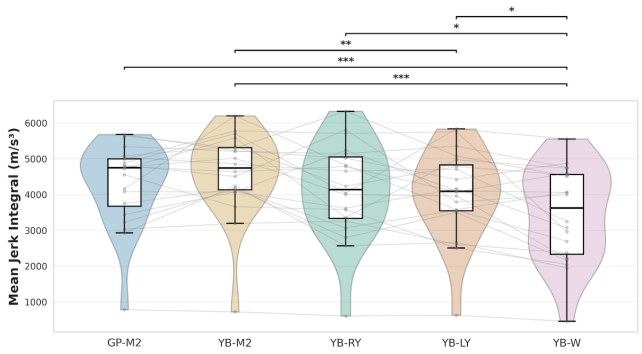


**Figure 6: Jerk integral for each operation condition. Shows violin plots and box plots, as well as trajectories for each participant.**

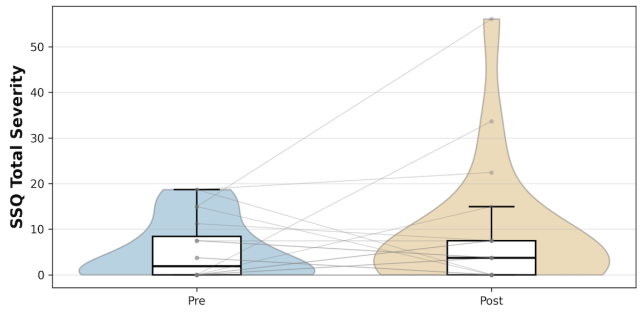


**Figure 7: SSQ Total Severity scores before and after the experiment. Shows violin plots and box plots, as well as trajectories for each participant.**

($W = 0.83$, $p = .003$). Wilcoxon signed-rank test showed no significant difference before and after the experiment, $V = 44$, $p = .373$, $r = 0.20$. Results are shown in Figure 7.

## 4.5 VEQ (Virtual Embodiment Questionnaire)

We used Agency items from the Virtual Embodiment Questionnaire (VEQ) [24] to evaluate the sense of embodiment for operation in each operation condition. We calculated mean scores for each participant in each operation condition. Shapiro-Wilk test confirmed normality for all conditions (all $p > .05$). Paired t-tests with Shaffer correction revealed: YB-M2 ($M = 2.84$, $SD = 1.19$) < YB-W ($M = 5.05$, $SD = 1.33$, $t(19) = -6.78$, $p < .001$, $d = -1.52$), GP-M2 ($M = 4.88$, $SD = 1.21$) > YB-M2 ($t(19) = 6.15$, $p < .001$, $d = 1.38$), YB-M2 < YB-LY ($M = 4.20$, $SD = 1.37$, $t(19) = -4.31$, $p = .002$, $d = -0.96$), YB-M2 < YB-RY ($M = 4.44$, $SD = 1.44$, $t(19) = -4.17$, $p = .003$, $d = -0.93$). Results are shown in Figure 8.

## 4.6 NASA-TLX

We used the localized version of NASA-TLX to evaluate subjective workload in each operation condition. We compared the six

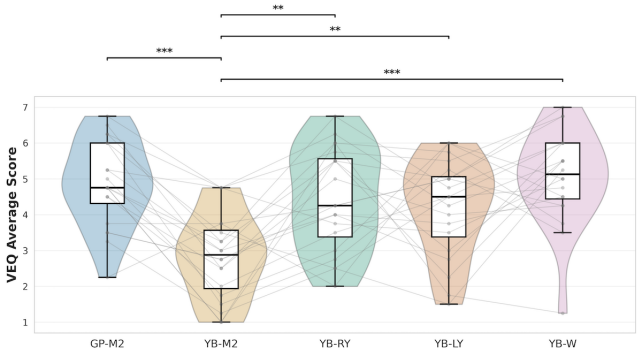


**Figure 8: Mean VEQ scores for each operation condition. Shows violin plots and box plots, as well as trajectories for each participant.**

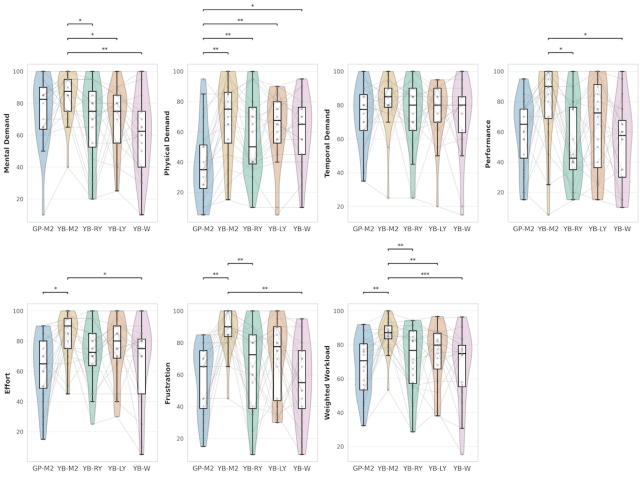


**Figure 9: NASA-TLX item scores for each operation condition. Shows distributions for each operation condition for Mental Demand, Physical Demand, Temporal Demand, Performance, Effort, Frustration, and Weighted Workload.**

items—Mental Demand, Physical Demand, Temporal Demand, Performance, Effort, and Frustration—and weighted Weighted Workload across operation conditions. Shapiro-Wilk test rejected normality for multiple items, so we used non-parametric tests. Wilcoxon signed-rank tests with Shaffer correction revealed the following significant results: Mental Demand: YB-M2 > YB-W ($p$ = .003), YB-M2 > YB-LY ($p$ = .011), YB-M2 > YB-RY ($p$ = .014); Physical Demand: GP-M2 < YB-M2 ($p$ = .003), GP-M2 < YB-RY ($p$ = .004), GP-M2 < YB-LY ($p$ = .006), GP-M2 < YB-W ($p$ = .022); Performance: YB-M2 > YB-RY ($p$ = .018), YB-M2 > YB-W ($p$ = .027); Effort: GP-M2 < YB-M2 ($p$ = .040), YB-M2 > YB-W ($p$ = .044); Frustration: YB-M2 > YB-W ($p$ = .004), GP-M2 < YB-M2 ($p$ = .003), YB-M2 > YB-RY ($p$ = .005); Weighted Workload: GP-M2 < YB-M2 ($p$ = .001), YB-M2 > YB-W ($p$ < .001), YB-M2 > YB-LY ($p$ = .001), YB-M2 > YB-RY ($p$ = .009). Results are shown in Figure 9.

## 4.7 Interview

Semi-structured interviews were conducted after experiencing all operation conditions.

Regarding intuitiveness evaluation, 12 out of 20 participants selected YB-W (followed by 4 for YB-LY, 3 for YB-RY, 1 for GP-M2). Reasons for selecting YB-W included: “could do it without thinking about the operation method” (P2), “wheel metaphor is intuitive” (P3, P6, P16), “could do it without thinking” (P7, P10), “stable because inputs from both hands are averaged” (P16, P21). Regarding ease of operation, evaluations were divided: 8 for YB-W, 8 for GP-M2, 3 for YB-RY. Participants who selected GP-M2 emphasized device familiarity and operation certainty, saying “can input what I intended” (P3), “range of motion is clear” (P19), “controller was easier to operate” (P12).

Seventeen participants selected YB-M2 as the most difficult operation condition. Main reasons included: cross-axis interference causing unintended yaw rotation due to vertical movement and yaw rotation being on the same left hand (P6, P8, P11, P16), “trying to ascend causes yaw rotation” (P6, P9, P16), cognitive confusion such as “forward/backward and up/down get mixed up” (P10), and difficulty performing forward/backward force input independently as a force input device characteristic (P11, P12).

Regarding technical challenges with the force input system, multiple participants pointed out difficulty grasping force input magnitude (P6, P13, P19, P20), unintended input when relaxed (P6, P19, P20), and finger position displacement (P13, P17, P20). On the other hand, regarding learning effects, statements suggesting improvement through proficiency included “difficult to learn but once learned can be done unconsciously” (P5), “quite intuitive and easy to use once accustomed” (P17).

# 5 Discussion

This study systematically compared and evaluated five operation conditions (gamepad Mode 2 and four force input mappings) for 4DoF locomotion control using a fingertip force input system. Results from behavioral logs, subjective evaluations (SSQ, VEQ, NASA-TLX), and semi-structured interviews using a tunnel passing task revealed the following insights.

## 5.1 Input Mapping Design and Objective Performance

Tunnel pass count results showed clear differences between operation conditions. GP-M2 and YB-W had high success rates, while YB-M2 had the lowest success rate. This result indicates that mapping differences significantly affect task performance even with the same 4DoF output.

Particularly noteworthy is that YB-M2 scored significantly lower than all other force input conditions. This suggests that Mode 2 mapping, which is standard for drone operation, is insufficient for fingertip force input devices without adaptation. In interviews, 17 participants rated YB-M2 as “most difficult,” repeatedly pointing out cross-axis interference between vertical movement and yaw rotation, and occurrence of unintended movements.

This YB-M2 problem is likely due to several critical differences between force input and joystick input. First, there may be a mismatch between users’ intuitive perception of input direction and

the actual output mapping. Joysticks are physically constrained to two-dimensional tilt, so users naturally accept that forward tilt corresponds to ascending. YUBI, however, can sense three-dimensional force vectors including vertical forces, so users may implicitly expect that pushing upward would produce upward movement. The horizontal-to-vertical mapping thus feels unintuitive for YUBI, as it ignores the device's structural capability for direct directional input. Second, joysticks possess multiple mechanisms that suppress unintended input, none of which were present in our force input implementation. Joystick input is displacement-based, and proprioceptive feedback from finger joint movement makes it relatively easy to isolate input along individual axes; force input is isometric, so force components inevitably arise in unintended directions. Moreover, the axis directions that users perceive may not align with the device's actual coordinate axes—for instance, a user may believe they are pushing straight down, but the device registers the force as slightly off-axis, generating unintended input components. Commercial joysticks also incorporate dead zones around the neutral position and non-linear input curves that reduce sensitivity near the center, absorbing small unintended deflections—even joysticks can exhibit drift if the dead zone is set to zero. Without these mechanisms, cross-axis force leakage, user-device axis misalignment, and minor residual forces when attempting to relax were all directly translated into movement commands. This is particularly problematic in YB-M2, where vertical movement and yaw rotation are assigned to different axes of the same hand; interviews confirmed that participants "cannot perform forward/backward movement independently from left/right movement" (P12) and found it "difficult to perform only push-pull operations independently" (P11). These differences explain why the same Mode 2 mapping yielded drastically different task performance between GP-M2 and YB-M2. However, these issues could be mitigated by introducing dead zones, non-linear input curves, and per-user calibration of input-output direction mappings. Notably, such engineering improvements are not specific to YB-M2 but could benefit all force input conditions, potentially elevating overall performance beyond what was observed in the present study.

In contrast, YB-W showed high success rates with no significant difference from GP-M2, the shortest completion time, and the smoothest movement (lowest jerk integral) among all conditions. YB-W is designed to use forward/backward force input from both hands integrally, controlling yaw rotation by the difference in left/right inputs. This approach leverages the problem of left/right component mixing in forward/backward force input, deliberately incorporating it as intentional left/right differences for yaw rotation control. Interviews yielded positive evaluations such as "stable because inputs from both hands are averaged" (P16) and "easy to stop yaw rotation because you just apply the same force with both hands" (P8).

Regarding task completion time, YB-W showed the shortest completion time with significant differences from GP-M2 and YB-RY. Jerk integral results also confirmed that YB-W showed significantly lower values compared to all other conditions, achieving smoother movement. This low jerk in YB-W may be partly attributed to the averaging effect of bilateral input: because both hands contribute to translational control, unintended force fluctuations from one hand could be partially canceled by the other, potentially resulting in smoother acceleration profiles. Additionally, YB-W's mapping may reduce the need for abrupt corrective inputs caused by cross-axis interference, which likely contributes to high jerk in YB-M2.

## 5.2 Subjective Workload and Embodiment

NASA-TLX results were consistent with objective performance results. YB-M2 showed significantly higher load than other conditions in Mental Demand, Performance, Effort, Frustration, and Weighted Workload. Cognitive confusion was also reported in interviews, confirming that YB-M2 demands high cognitive load.

For Physical Demand, GP-M2 was significantly lower than all force input conditions. This indicates that joystick operation is less physically demanding than force input. Although we normalized input gains so that 1.4N of force was equivalent to fully tilting the joystick, force input consistently required higher physical effort. This discrepancy likely stems from a fundamental difference in input constraints: joysticks have a clear physical limit—users can feel when the stick reaches its maximum tilt, providing unambiguous feedback about maximum input. In contrast, force input devices have no such physical limit; users cannot directly perceive when they have reached the force threshold. This lack of physical boundary may lead users to apply excessive force beyond what is necessary, resulting in higher physical demand despite equivalent input-output mappings.

For VEQ Agency items, YB-M2 showed significantly lower scores than all other conditions, indicating participants felt less physical control and sense of agency over operations in YB-M2. This suggests that cross-axis interference and occurrence of unintended movements in YB-M2 impaired the sense of embodiment for operation.

In interviews, 12 out of 20 participants rated YB-W as "most intuitive." Participants cited reasons such as "wheel metaphor is intuitive" (P3, P6, P16), "symmetrical so don't need to think" (P12), and "could do it without thinking" (P7, P10), suggesting that correspondence with existing mental models (wheels, cars, karts, etc.) contributed to intuitiveness.

## 5.3 Individual Differences in Ease of Operation and Learning Effects

As reported in the interview results, evaluations of "ease of operation" were divided between YB-W and GP-M2, indicating that objective performance and subjective ease of operation do not necessarily match. Participants who preferred GP-M2 emphasized device familiarity and operation certainty, suggesting that existing familiarity with game controllers remains important for some users.

Regarding force input learning effects, several participants suggested that performance improves substantially after an initial learning period, indicating the force input system has potential for more intuitive and efficient operation with practice. Additionally, we did not provide a learning phase for the force input system itself, and with only 36 trials per operation condition, we may not have adequately evaluated long-term learning effects.

## 5.4 Simulator Sickness

SSQ results showed no significant change in simulator sickness level before and after the experiment. This indicates that severe simulator

sickness did not occur in this experiment's tasks and duration (approximately 90 minutes). Using a standard display monitor may have contributed to suppressing simulator sickness.

## 5.5 Challenges with Force Input Devices

This study also revealed operational challenges specific to force input devices. Issues repeatedly pointed out in interviews include difficulty grasping force input magnitude, unintended input when relaxed, and finger position displacement. In joysticks, physical displacement provides visual and tactile feedback, but force input devices lack displacement, making it difficult to grasp input magnitude. Furthermore, the absence of a physical limit in force input (unlike joysticks that have a clear maximum tilt) makes it difficult for users to determine when they have reached maximum input, potentially leading to excessive force application. Additionally, without dead zones or non-linear input curves that commercial joysticks incorporate, even minor residual forces are registered as input, making stable zero-point maintenance challenging. These issues suggest the need for countermeasures such as adding visual force feedback, providing clearer indicators of force thresholds, introducing dead zones and non-linear input curves to improve zero-point stability, per-user calibration of input-output direction alignment, and improving attachment methods.

## 5.6 Implications for 3D Locomotion Interface Design

The results of this study provide the following implications for designing 3D locomotion control interfaces:

First, directly applying the standard joystick mapping (Mode 2) to force input devices without adaptation is insufficient. Input mapping design must account for the mismatch between users' intuitive input directions and the mapping's expected directions, as well as the lack of unintended input suppression mechanisms such as dead zones and non-linear input curves that commercial joysticks incorporate. However, incorporating these mechanisms along with per-user calibration of input-output direction alignment may mitigate these issues, leaving open the possibility that adapted Mode 2-style mappings could perform better than observed in this study.

Second, integrated control using real-world metaphors (YB-W) can leverage the problem of cross-axis interference in force input to realize effective operation interfaces. Using inputs from both hands integrally enables stable and smooth control, and leveraging mental models users already possess reduces learning costs and improves operation intuitiveness and embodiment.

Third, force input devices require an initial learning period but may exhibit high operability after proficiency. For practical application, designing appropriate learning phases and tutorials is important.

Finally, addressing technical challenges such as force input magnitude feedback, zero-point maintenance, and ergonomics is essential for improving force input device practicality.

## 5.7 Limitations

This study has several limitations. First, we used a standard display monitor rather than VR head-mounted displays, limiting immersion and depth perception. Additionally, no background or reference points were set in the 3D virtual space, making it difficult to grasp self-position when losing sight of tunnels. Future evaluation in more immersive VR environments is needed to fully assess force input advantages in 3D space.

Second, with only 36 trials per operation condition, evaluation of long-term learning effects was insufficient. Interview suggestions such as "difficult to learn but once learned can be done unconsciously" (P5) indicate potential for improved performance with extended practice. Additionally, while Latin square design was used for counterbalancing, cross-condition learning effects (e.g., familiarity with physical simulation parameters) could not be fully separated. However, consistent subjective evaluations across presentation orders—with 17/20 participants rating YB-M2 as "most difficult" and 12/20 rating YB-W as "most intuitive"—suggest that observed differences reflect genuine mapping characteristics rather than order effects.

Third, YB-W utilizes 6DoF input (3DoF per thumb) to control 4DoF locomotion, whereas other conditions use only 4DoF input. This redundancy is a key design feature that enables averaging to mitigate cross-axis interference, but it also means that the performance advantage of YB-W cannot be attributed solely to the mapping strategy; the additional input dimensions may also contribute. Future studies should isolate the effects of redundancy and mapping design.

Finally, this study evaluated only one specific fingertip force input device. Generalization to other force input devices (e.g., 3D mouse, different form factors) requires further investigation. Additionally, participants' existing familiarity with game controllers may have advantaged GP-M2. Nevertheless, YB-W achieved comparable success rates and shorter completion times despite participants' first-time use of the force input device, demonstrating the potential effectiveness of appropriate force input mappings.

# 6 Conclusion

This study compared five operation conditions for 4DoF locomotion control in a 3D tunnel-passing task: gamepad Mode 2 and four force input mappings. First, directly applying conventional joystick mappings (Mode 2) to force input devices without adaptation is insufficient. YB-M2 showed the lowest success rate and highest workload, likely due to the mismatch between users' intuitive input directions and the mapping, and the absence of unintended input suppression mechanisms such as dead zones and non-linear input curves. These issues may be mitigated through per-user calibration and appropriate input processing. Second, integrated control using real-world metaphors (wheel-based mapping) can leverage force input characteristics to realize effective interfaces. YB-W achieved comparable success rates to GP-M2, the shortest completion time, and highest intuitiveness ratings (12/20 participants). This demonstrates that force input devices can achieve comparable task performance to gamepads and high intuitiveness when paired with appropriate mappings that leverage existing mental models and account for unique device characteristics such as the difficulty in axis separation inherent to isometric input and the lack of automatic centering. These insights contribute to designing 3D locomotion interfaces for applications such as drone operation, VR navigation,

and teleoperation. Moreover, because fingertip force input enables compact, wearable control with minimal physical displacement, it can further extend to assistive mobility control for users with physical constraints, and VR locomotion where thumbs handle movement while remaining fingers perform other interaction tasks. Future work should evaluate long-term learning effects, VR environments, and more complex operational tasks, as well as the impact of engineering refinements such as dead zones, non-linear input curves, and per-user calibration of input-output direction alignment on force input performance.

## Acknowledgments

This work was partially supported by JST Moonshot Research & Development Program (JPMJMS2013) and Grant-in-Aid for Early-Career Scientists (24K20818, 25K21242).

## References

[1] Jessica R. Cauchard, Jane L. E, Kevin Y. Zhai, and James A. Landay. 2015. Drone & me: an exploration into natural human-drone interaction. In *Proceedings of the 2015 ACM International Joint Conference on Pervasive and Ubiquitous Computing* (Osaka, Japan) *(UbiComp '15)*. Association for Computing Machinery, New York, NY, USA, 361–365. doi:10.1145/2750858.2805823

[2] Weiya Chen, Anthony Plancoulaine, Nicolas Férey, Damien Touraine, Julien Nelson, and Patrick Bourdot. 2013. 6DoF navigation in virtual worlds: comparison of joystick-based and head-controlled paradigms *(VRST '13)*. Association for Computing Machinery, New York, NY, USA, 111–114. doi:10.1145/2503713.2503754

[3] Hee-Wook Choi, Hyung-Jin Kim, Sung-Keun Kim, and Wongi S. Na. 2023. An Overview of Drone Applications in the Construction Industry. *Drones* 7, 8 (2023). doi:10.3390/drones7080515

[4] R.A. Cooper, D.K. Jones, S. Fitzgerald, M.L. Boninger, and S.J. Albright. 2000. Analysis of position and isometric joysticks for powered wheelchair driving. *IEEE Transactions on Biomedical Engineering* 47, 7 (2000), 902–910. doi:10.1109/10.846684

[5] Yuran Ding, Nihar Sabnis, and Paul Strohmeier. 2024. Motionless movement: Towards vibrotactile kinesthetic displays. In *Proceedings of the CHI Conference on Human Factors in Computing Systems*, Vol. 16. ACM, New York, NY, USA, 1–16. doi:10.1145/3613904.3642499

[6] Shigeru Haga and Naoki Mizukami. 1996. Japanese version of nasa task load index sensitivity of its workload score to difficulty of three different laboratory tasks. *The Japanese journal of ergonomics* 32, 2 (1996), 71–79.

[7] John Paulin Hansen, Alexandre Alapetite, I. Scott MacKenzie, and Emilie Møllenbach. 2014. The use of gaze to control drones. In *Proceedings of the Symposium on Eye Tracking Research and Applications* (Safety Harbor, Florida) *(ETRA '14)*. Association for Computing Machinery, New York, NY, USA, 27–34. doi:10.1145/2578153.2578156

[8] Abraham M. Hashemian, Matin Lotfaliei, Ashu Adhikari, Ernst Kruijff, and Bernhard E. Riecke. 2022. HeadJoystick: Improving Flying in VR Using a Novel Leaning-Based Interface. *IEEE Transactions on Visualization and Computer Graphics* 28, 4 (2022), 1792–1809. doi:10.1109/TVCG.2020.3025084

[9] Takeru Hashimoto and Yutaro Hirao. 2024. Selfrionette: A Fingertip Force-Input Controller for Continuous Full-Body Avatar Manipulation and Diverse Haptic Interactions. In *Proceedings of the 37th Annual ACM Symposium on User Interface Software and Technology*. 1–14.

[10] Keita Higuchi, Katsuya Fujii, and Jun Rekimoto. 2013. Flying head: A head-synchronization mechanism for flying telepresence. In *2013 23rd International Conference on Artificial Reality and Telexistence (ICAT)*. 28–34. doi:10.1109/ICAT.2013.6728902

[11] Yutaro Hirao and Takeru Hashimoto. 2025. A Demonstration of YUBI: Your Universal Body Interface Using Finger Force to Full-Body Motion for Avatar Embodiment. In *ACM SIGGRAPH 2025 Emerging Technologies (SIGGRAPH '25)*. Association for Computing Machinery, New York, NY, USA, Article 1, 2 pages. doi:10.1145/3721257.3743094

[12] Kohki Ikeuchi, Tomoaki Otsuka, Akihito Yoshii, Mizuki Sakamoto, and Tatsuo Nakajima. 2014. KinecDrone: enhancing somatic sensation to fly in the sky with Kinect and AR.Drone. In *Proceedings of the 5th Augmented Human International Conference* (Kobe, Japan) *(AH '14)*. Association for Computing Machinery, New York, NY, USA, Article 53, 2 pages. doi:10.1145/2582051.2582104

[13] T Imanaga, N Mochizuki, N Okamoto, and others. 2022. Research on Motion-Less VR: Comparison of Muscle Outputs Between Motion Using Developed System and Natural Motion. *2022 IEEE/SICE* (2022).

[14] Robert S Kennedy, Norman E Lane, Kevin S Berbaum, and Michael G Lilienthal. 1993. Simulator sickness questionnaire: An enhanced method for quantifying simulator sickness. *The international journal of aviation psychology* 3, 3 (1993), 203–220.

[15] Konstantoudakis Konstantinos, Christaki Kyriaki, Tsiakmakis Dimitrios, Sainidis Dimitrios, Albanis Georgios, Dimou Anastasios, and Daras Petros. 2022. Drone Control in AR: An Intuitive System for Single-Handed Gesture Control, Drone Tracking, and Contextualized Camera Feed Visualization in Augmented Reality. *Drones* 6, 2 (02 2022), 43. doi:10.3390/drones6020043

[16] Yang Li, Rintaro Iio, Shoun Nishioka, Tatsuro Terakawa, and Masaharu Komori. 2025. Analysis of Force Characteristics in Foot Operations Using Isometric Device. *IEEE Access* 13 (2025), 71197–71213. doi:10.1109/ACCESS.2025.3562377

[17] Ahmed Mashood, Hassan Noura, Imad Jawhar, and Nader Mohamed. 2015. A gesture based kinect for quadrotor control. In *2015 International Conference on Information and Communication Technology Research (ICTRC)*. 298–301. doi:10.1109/ICTRC.2015.7156481

[18] Jenifer Miehlbradt, Alexandre Cherpillod, Stefano Mintchev, Martina Coscia, Fiorenzo Artoni, Dario Floreano, and Silvestro Micera. 2018. Data-driven body–machine interface for the accurate control of drones. *Proceedings of the National Academy of Sciences* 115, 31 (2018), 7913–7918. doi:10.1073/pnas.1718648115 arXiv:https://www.pnas.org/doi/pdf/10.1073/pnas.1718648115

[19] Mani Monajjemi, Sepehr Mohaimenianpour, and Richard Vaughan. 2016. UAV, come to me: End-to-end, multi-scale situated HRI with an uninstrumented human and a distant UAV. In *2016 IEEE/RSJ International Conference on Intelligent Robots and Systems (IROS)*. 4410–4417. doi:10.1109/IROS.2016.7759649

[20] Tayyab Naseer, Jürgen Sturm, and Daniel Cremers. 2013. FollowMe: Person following and gesture recognition with a quadrocopter. In *2013 IEEE/RSJ International Conference on Intelligent Robots and Systems*. 624–630. doi:10.1109/IROS.2013.6696416

[21] Wai Shan Ng and Ehud Sharlin. 2011. Collocated interaction with flying robots. In *2011 RO-MAN*. 143–149. doi:10.1109/ROMAN.2011.6005280

[22] Masataka Niwa, Shinya Okada, Shota Sakaguchi, Kentaro Azuma, Hiroyuki Iizuka, Hideyuki Ando, and Taro Maeda. 2010. Detection and transmission of "tsumori": an archetype of behavioral intention in controlling a humanoid robot. In *Proceeding of 20th International Conference on Artificial Reality and Telexistance (ICAT2010)*. 197–201.

[23] Kevin Pfeil, Seng Lee Koh, and Joseph LaViola. 2013. Exploring 3d gesture metaphors for interaction with unmanned aerial vehicles. In *Proceedings of the 2013 International Conference on Intelligent User Interfaces* (Santa Monica, California, USA) *(IUI '13)*. Association for Computing Machinery, New York, NY, USA, 257–266. doi:10.1145/2449396.2449429

[24] Daniel Roth and Marc Erich Latoschik. 2020. Construction of the virtual embodiment questionnaire (veq). *IEEE Transactions on Visualization and Computer Graphics* 26, 12 (2020), 3546–3556.

[25] Ayanava Sarkar, Ketul Arvindbhai Patel, R.K. Ganesh Ram, and Geet Krishna Capoor. 2016. Gesture control of drone using a motion controller. In *2016 International Conference on Industrial Informatics and Computer Systems (CIICS)*. 1–5. doi:10.1109/ICCSII.2016.7462401

[26] Alexandru-Ionut Siean. 2024. SkySculptor: Intuitive Drone Control Through Ground-Integrated Radar and Foot Gestures in Smart Indoor Environments. *International Journal of Advanced Computer Science and Applications* 15, 2 (2024). doi:10.14569/IJACSA.2024.0150204

[27] Adrian Stoica, Federico Salvioli, and Caitlin Flowers. 2014. Remote Control of Quadrotor Teams, Using Hand Gestures. In *2014 9th ACM/IEEE International Conference on Human-Robot Interaction (HRI)*. 296–297.

[28] João Marcelo Teixeira, Ronaldo Ferreira, Matheus Santos, and Veronica Teichrieb. 2014. Teleoperation Using Google Glass and AR, Drone for Structural Inspection. In *2014 XVI Symposium on Virtual and Augmented Reality*. 28–36. doi:10.1109/SVR.2014.42